https://doi.org/10.5194/acp-2021-457
Preprint. Discussion started: 27 July 2021

Atmospheric Chemistry and Physics Discussions

Measurement report: Vehicle-based and In Situ Multi-lidar Observational Study on the Effect of Meteorological Elements on the Three-dimensional Distribution of Particles in the Western Guangdong–Hong Kong–Macao Greater Bay Area

Xinqi Xu[1,2], Jielan Xie[1,2], Yuman Li[1,2], Shengjie Miao[1,2], and Shaojia Fan[1,2]

[1]School of Atmospheric Sciences, Sun Yat-sen University, Zhuhai, 519082, China
[2]Guangdong Provincial Observation and Research Station for Climate Environment and Air Quality Change in the Pearl River Estuary, Key Laboratory of Tropical Atmosphere-Ocean System, Ministry of Education, Southern Marine Science and Engineering Guangdong Laboratory (Zhuhai), Zhuhai, 519082, China

Correspondence to: Shaojia Fan (eesfsj@mail.sysu.edu.cn)

Abstract: The distribution of meteorological elements has always been an important factor in determining the horizontal and vertical distribution of particles in the atmosphere. To study the effect of meteorological elements on the three-dimensional distribution structure of particles, mobile vehicle lidar observations, and in situ observations were presented in the western Guangdong–Hong Kong–Macao Greater Bay Area of China during September and October of 2019 and 2020. Vertical aerosol extinction coefficient, depolarization ratio, wind and temperature profiles were measured by using a micro pulse lidar, a Raman scattering lidar, and a Doppler wind profile lidar installed on a mobile monitoring vehicle. The mechanism of how wind and temperature in the boundary layer affects the horizontal and vertical distribution of particles was analyzed. The result showed that particles were mostly distributed in downstream areas on days with moderate wind speed in the boundary layer, while they presented homogeneously on days with weaker wind. There are three typical types of vertical distribution of particles in the western Guangdong–Hong Kong–Macao Greater Bay Area (GBA): surface single layer, elevated single layer, and double layer. Analysis of wind profiles and Hybrid Single-Particle Lagrangian Integrated Trajectory Model（HYSPLIT) backward trajectory revealed different sources of particles for the three types. Particles concentrated near the temperature inversion and multiple inversions could cause more than one peak in the extinction coefficient profile. There are two mechanisms that affected the distribution of particulate matter in the upper and lower boundary layers. Based on observational study, a general model of meteorological elements affecting the vertical distribution of urban particulate matter was made.

1. Introduction

The Guangdong–Hong Kong–Macao Greater Bay Area (GBA) is one of China's national key economic development regions. It consists of Guangzhou (GZ), Shenzhen (SZ), Zhuhai (ZH), Foshan (FS), Huizhou (HZ), Dongguan (DG), Zhongshan (ZS), Jiangmen (JM), and Zhaoqing (ZQ) in Guangdong province, as well as Hong Kong and Macao, the two Special Administrative Regions.

https://doi.org/10.5194/acp-2021-457
Preprint. Discussion started: 27 July 2021

Covering 56,000 square kilometers, the GBA had a vast population of over 70 million at the end of 2018. The GBA plays a significant role in boosting global trade along the land-based Silk Road Economic Belt and the 21st Century Maritime Silk Road. With the rapid development of the regional economy, increasingly more studies on air quality and climate effect in the GBA have also been conducted (Fang et al., 2018; Shao et al., 2020; Zhou et al., 2018).

Anthophogenic particles in the air play an important role in the environment of human living. They not only act as air pollutants posing harmful effects to human health (Liao et al., 2017; Leikauf et al., 2020; Yao et al., 2020; Orru et al., 2017) but also alter the temperature near the ground owing to their ability to absorb and scatter solar radiation (IPCC, 2014; Strawa et al., 2010). As a result of industrialization and urbanization, megacity clusters in China such as the Beijing–Tianjin–Hebei [also called Jing-Jin-Ji (JJJ) in Chinese] area, Yangtze River Delta (YRD), and Guangdong–Hong Kong–Macao GBA, have been seriously affected by particulate matter in recent years. Numerous studies on the particulate matter have been conducted in these areas (Xu et al., 2018; Liu et al., 2017; Du et al., 2017). Particles in the boundary layer can, directly and indirectly, affect human lives and activities. Therefore, it is essential to study their distribution characteristics.

The distribution of particles is influenced not only by changes in source emissions but also by changes in meteorological factors, such as temperature and wind. For example, previous studies have confirmed that different types of temperature inversions have different impacts on particles in the boundary layer (Wallace et al., 2009; Zang et al., 2017). The concentration of particulate matter also shows characteristics of wind-dependent spatial distributions in which pollutant transport within the GBA city cluster is significant (Xie et al., 2019). Hence, the issue of how meteorological factors affecting the distribution of particles has received considerable critical attention.

Lidar is an active remote sensing device. It emits a laser light beam and receives a backscatter signal, which can be further used to retrieve vertical distribution of particle optical properties, as well as wind and temperature. It has been wildly applied in the fields of meteorology and environmental science. In most of the research, it was used as a ground-based or satellite-based instrument (Tian et al., 2016; Liu et al., 2017; Heese et al., 2017).

In recent years, vehicle-based lidar observation has gradually developed and become a powerful tool to detect the physical and chemical properties of the boundary layer. Compared with the traditional in situ observation, it can carry out continuous mobile observation and obtain the change of the vertical profiles of certain factors in the path. Additionally, it can be used as a mobile lidar system to conduct supplementary observation in areas with no lidar assembled. In the past few years, several vehicle-based observation experiments have been carried out (Lv et al., 2017; Lyu et al., 2018), but research aimed at multi-lidar observation and the effect of the vertical structure of meteorological factors to the distribution of particles had been a largely underexplored domain, especially in the GBA. The former research revealed that pollution of particulate matter frequently occurs in the western part of inland regions of GBA (Fang et al., 2019), affecting downstream cities under the northerly wind field. Hence, the authors were motivated to perform observations in the western GBA with a multi-lidar system installed on the vehicle to study the influence of the three-dimensional structure of meteorological elements on the distribution of particles.

https://doi.org/10.5194/acp-2021-457
Preprint. Discussion started: 27 July 2021

Atmospheric Chemistry and Physics
Discussions

2. Data and Method

2.1 Description of Observations

The horizontal distribution of the particles was studied by making mobile vehicle lidar observations over the west bank of the Pearl River Estuary. During the mobile vehicle lidar observations experiment, the vehicle drove clockwise along the west bank of the Pearl River Estuary, passing through main cities of the GBA in the route, from as far north as Guangzhou to as far south as Zhuhai. The total length of the route was approximately 320 km, and the experiment was conducted during the daytime. The vehicle-based observation lasted for seven continuous days, which started on 29 August and ended on 4 September 2020. During most of the mobile observations, the relative humidity of Zhuhai, the closest city to the sea, was below 60 %. Therefore, the influence of hygroscopic growth on the extinction coefficient was negligible. To study the vertical distribution of the particles, in situ observations were made at Haizhu Lake Research Base in September and October of 2019 and 2020. The location of the Haizhu Lake Research Base and the area of the measuring path are shown in Fig. 1.

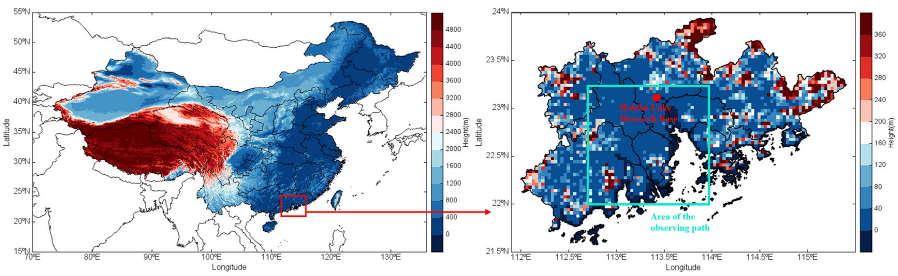

Figure 1: Location of the Haizhu Lake Research Base and area of the observation path.

2.2 Multi-lidar System

A multi-lidar system was installed on a vehicle in this experiment. The lidar system included a 3D visual scanning micro pulse lidar (EV-Lidar-CAM, EVERISE Company, Beijing, http://www.everisetech.com.cn/products/ygtc/evlidarportable.html), a twirling Raman temperature profile lidar (TRL20, EVERISE Company, Beijing, http://www.everisetech.com.cn/products/ygtc/templidar.html), a Doppler wind profile lidar (Windview10, EVERISE Company, Beijing, http://www.everisetech.com.cn/products/ygtc/windview10.html), a global positioning system (GPS), and a signal acquisition unit. The three lidars are characterized by high temporal and spatial resolution, and can effectively identify the evolution of the vertical distribution of particles, as well as temperature, wind speed, and wind direction over time. The details of the three lidars are shown in Table 1.

Table 1: Detailed parameters for three lidars.

Lidar	Variable	Laser source	Wave length	Laser frequency	Spatial resolution	Time resolution
Micro pulse lidar	Original signal, extinction coefficient	Nd:YAG	532 nm	2500 Hz	15 m	1 min

https://doi.org/10.5194/acp-2021-457
Preprint. Discussion started: 27 July 2021

	profiles, depolarization ratio profiles, Aerosol Optical Depth	laser				
Raman temperature profile lidar	Temperature profiles	Nd:YAG laser	532 nm	20 Hz	60 m	5 min
Doppler wind profile lidar	Wind speed profiles, Wind direction profiles	Fiber pulse laser	1545 nm	10 kHz	50 m	1 min

2.3 Calculation of Extinction Coefficient and Depolarization Ratio

The aerosol extinction coefficient represents the reduction of radiation in a band owing to scattering and absorption by aerosols (Li et al., 2020). The formula for the extinction coefficient calculation (Fernald, 1984) is as follows:

$$\alpha_a(z) = -\frac{S_a}{S_m}\alpha_m(z) + \frac{P(z)z^2 \cdot \exp\left[2\left(\frac{S_a}{S_m}-1\right)\int_z^{z_c}\alpha_m(z)\mathrm{d}z\right]}{\frac{P(z_c)z^2}{\alpha_a(z_c)+\frac{S_a}{S_m}\alpha_m(z_c)}+2\int_z^{z_c}P(z)z^2\exp\left[2\left(\frac{S_a}{S_m}-1\right)\int_z^{z_c}\alpha_m(z)\mathrm{d}z\right]\mathrm{d}z} \tag{1}$$

where $P(z)$ is the power received at altitude z; α_a and α_m denote particle extinction and molecular extinction, respectively. $S_a = 50$ Sr is the particle extinction-to-backscatter ratio. $S_m = 8\pi/3$ is the molecular extinction-to-backscatter ratio. z_c is the calibration height of the micro pulse lidar.

The micro pulse lidar (MPL) system uses the scattering of polarized light to distinguish between spherical and nonspherical particles to ascertain the particle species (Li et al., 2020). The depolarization ratio is calculated with the following formula:

$$\delta = k\frac{P_\perp}{P_\parallel} \tag{2}$$

where $P_\perp$ and $P_\parallel$ represent the cross-polarized and co-polarized signal, respectively.

2.4 HYSPLIT Backward Trajectory Model

The regional transport of particulate matter was studied using the National Oceanic and Atmospheric Administration Hybrid Single-Particle Lagrangian Integrated Trajectory Model (HYSPLIT) so as to determine the trajectory of air masses. It has been widely used in the field of air masses and pollutant source analysis (Deng et al., 2016; Lu et al., 2018; Kim et al., 2020). In this study, to obtain the sources of particulate matter at different heights, altitudes of 100 m, 500 m, and 1000 m were set as the ending points of the trajectories.

https://doi.org/10.5194/acp-2021-457
Preprint. Discussion started: 27 July 2021

3. Results and Discussion

3.1 Mobile Vehicle Lidar Observations

The horizontal distribution of particles was obtained by conducting mobile vehicle lidar observations in the GBA. Figure 2 shows the aerosol optical depth (AOD) measured with the MPL in the route. Because of GPS signal interference, some GPS data on 31 August and 2 September were missing. On most days, sections with high AOD values fell geographically into the south and west sides of the observation region. Figure 3 demonstrates low-level horizontal wind fields on 925 hPa over the region based on ERA5 reanalysis data. In the first three days, the wind speed over the GBA was generally higher, and the wind direction was easterly and northeasterly. Polluted aerosols were transported along with the wind to the west and south of the area. They accumulated in the downstream area, resulting in a high value of AOD. On 1, 3, and 4 September, the GBA was in the area of low wind speed, which was not conducive to the regional transport of particulate matter. As a result, the AOD value of the whole GBA reached a higher level, of which the increase of AOD in the northern region was more obvious. AOD values on these days distributed more homogenously than days with higher wind speed. On 2 September, the lower winds of the GBA turned westerly when the observation area in the east was downstream, and the highest points of the AOD value also appeared on the eastern route. Such results show that the horizontal distribution of particles in the GBA was closely related to wind speed and wind direction.

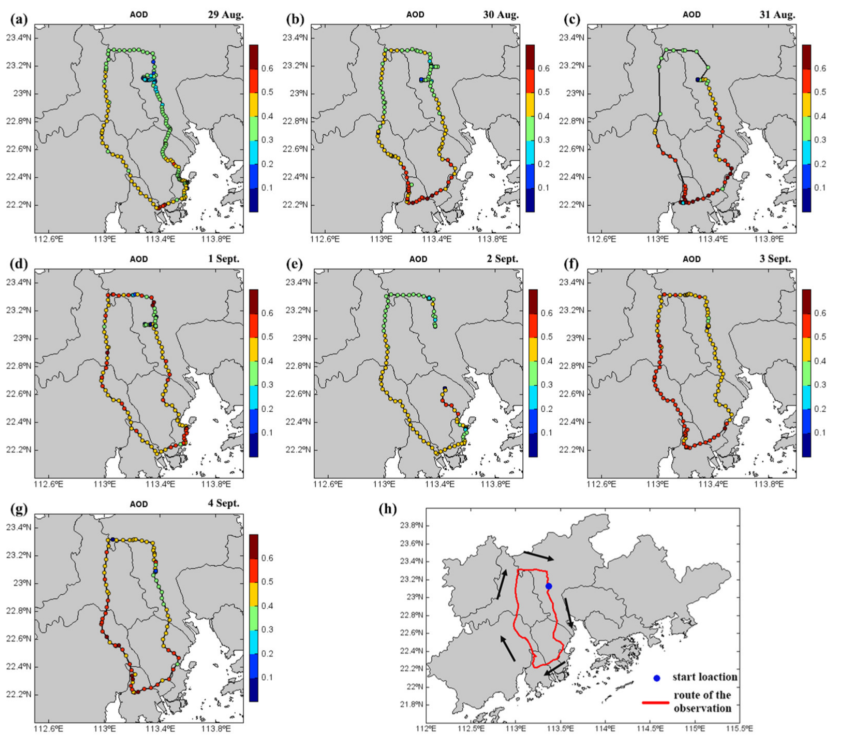

Figure 2. (a)-(g) Aerosol optical depth (AOD) measured with the MPL in the route from 29 August to 4 September 2020 and (h) Guangdong–Hong Kong–Macao Greater Bay Area and details of the route.

https://doi.org/10.5194/acp-2021-457
Preprint. Discussion started: 27 July 2021

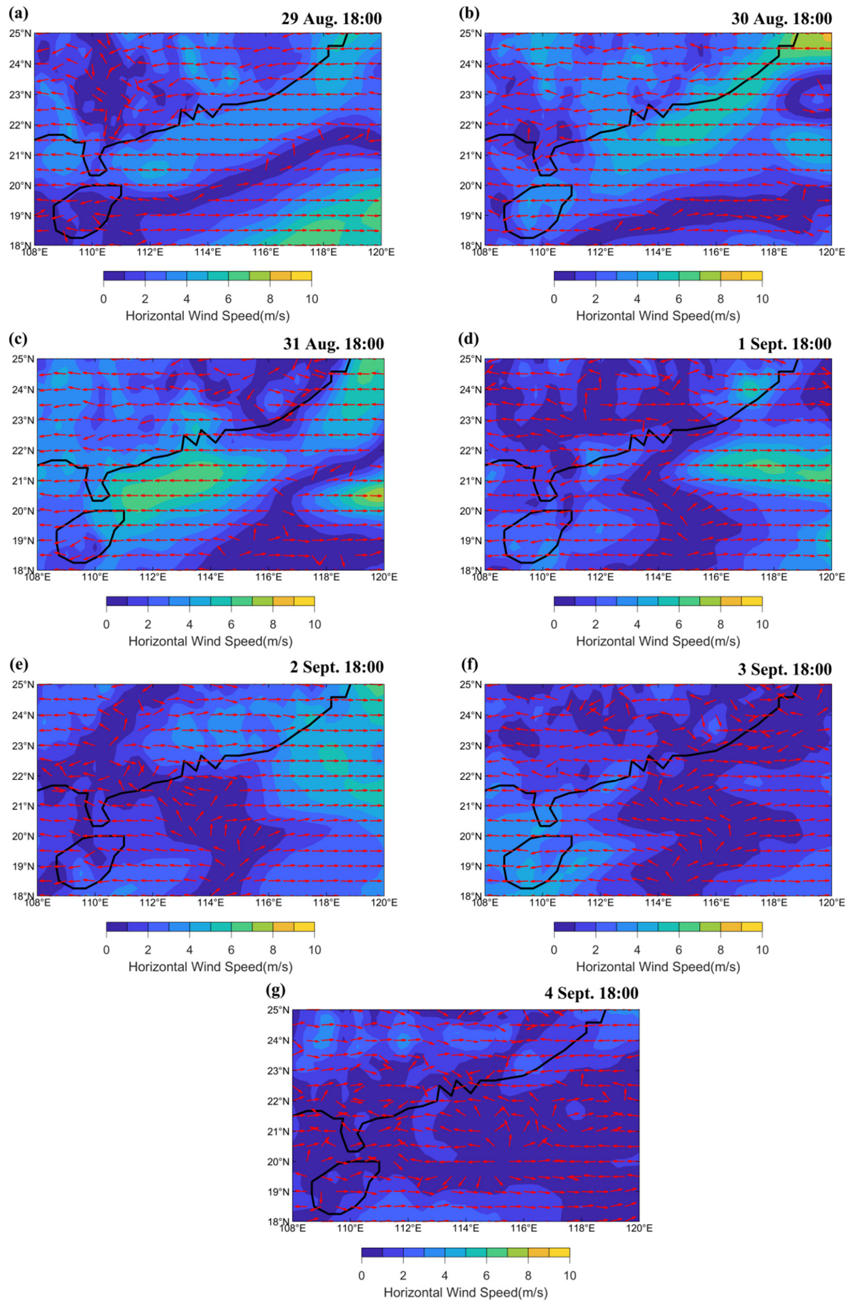

Figure 3. (a)-(g) Wind field of 925 hPa from 29 August to 4 September 2020. The color map represents horizontal wind speed (m/s). Red arrows represent the wind direction.

https://doi.org/10.5194/acp-2021-457
Preprint. Discussion started: 27 July 2021

3.2 In Situ Lidar Observations

To obtain the vertical distribution of particles, in situ lidar observations were conducted at the Haizhu Lake Research Base in Guangzhou, which could typically represent the situation of the GBA. As daytime temperatures in the GBA were still high in September and October, the development of the convective boundary layer during the day was vigorous, making it conducive to particle diffusion. Therefore, the value of the extinction coefficient near the ground during the day was generally low. The hierarchical structure of aerosols occurred more frequently at night. Three different vertical distribution types of particles are given below, as well as the corresponding vertical observation results of temperature and wind in the same period.

3.2.1 Type I: Surface Single Layer

On 3 September 2020, a clear night in autumn, the lidar system operated from 2154 to 0609 local time (LT) the next day. Figure 4(a) shows the time series of the extinction coefficient of a single aerosol layer on the surface, which was observed with the MPL. Before 0300 LT, particles accumulated below 800 m. The maximum value of the extinction coefficient near the ground was between 0.3–0.5. During 0300 LT and 0400 LT, there is a significant increase in the maximum height of the particle layer. After 0430 LT, the maximum height of the particle layer dropped, and the near-ground extinction coefficient fell below 0.3. Figure 4(b) shows the time series of corresponding depolarization ratio profiles. Most of the depolarization ratios were below 0.1, consistent with previous research on the GBA (Tian et al., 2017). A layer of elevated depolarization ratio was visible near the boundary of the surface single layer in Fig. 3(a). It can be seen that during 0300 LT and 0400 LT, there was a significant hierarchical structure with a high depolarization ratio layer near the ground and another layer of high value above. A layer with a lower value of depolarization ratio existed between the two layers with a higher value. This result indicated that there might be local anthropogenic emissions during the period.

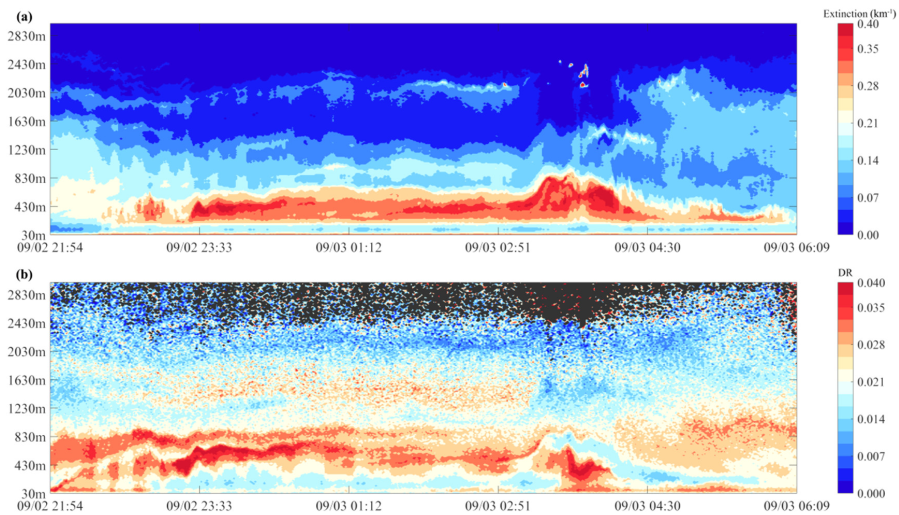

Figure 4. Extinction coefficient at 532 nm (a) and depolarization ratio (b) from 2154 LT 02 on September 2020 to 0609 LT on 03 September 2020.

https://doi.org/10.5194/acp-2021-457
Preprint. Discussion started: 27 July 2021

Figure 5 shows the horizontal wind speed and wind direction over the observation points in this period. Noticeably, a calm wind layer appeared below 1000 m, with horizontal wind speeds of each height maintained below 2 m/s. Such a static and stable condition was advantageous to the accumulation of locally generated particulate matter near the ground. However, it acted as a disincentive to the regional transport of particulate matter at a higher altitude. Therefore, when calm wind dominated near the ground, the particulate matter was likely to form a single layer on the surface.

It is worth noting that the wind at an altitude of 540 m at night gradually shifted to southerly wind, while the northerly weight of the 290 m altitude wind gradually increased. This shift in the wind was typical of a sea-land breeze in nocturnal coastal areas, which can only be observed when the background wind speed was relatively low.

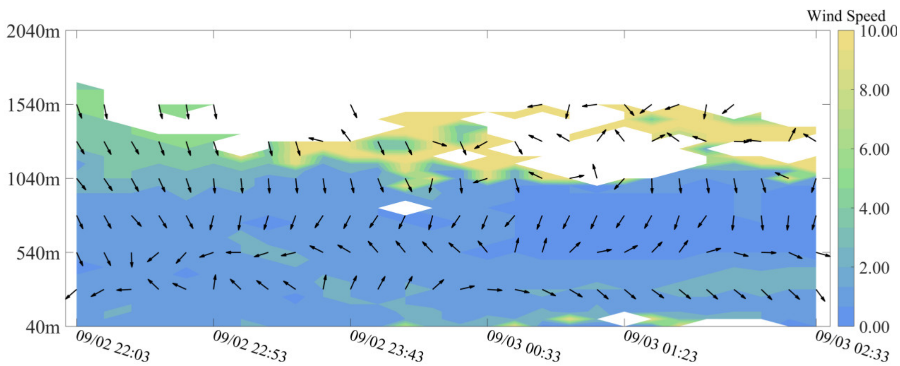

Figure 5. Wind speed and wind direction of Type I. The color map represents horizontal wind speed (m/s). Arrows represents the wind direction.

The backward trajectories analysis of the same period (Figure 6) shows that on a large scale, the airflow in the boundary layer came from the north. The vertical trajectories of each layer were roughly parallel within 24 h, and all traveled from high altitude to low, suggesting that particulate matter emitted near the ground in neighboring cities was not easily transported by wind to Guangzhou.

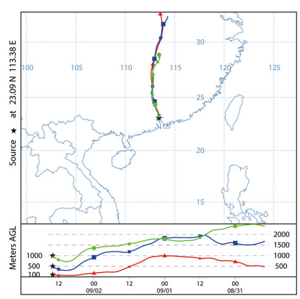

Figure 6. Backward trajectories at 100 m, 500 m, and 1000 m, ending at 2200 LT 02 September 2020, determined by the HYSPLIT model.

Observations from the Raman temperature profile lidar (Figure 7) show an inversion between 600–

https://doi.org/10.5194/acp-2021-457
Preprint. Discussion started: 27 July 2021

Atmospheric Chemistry and Physics
Discussions

1200 m before 0300 LT, which then rose to 1200 m and shrank to near the ground. Temperature inversion often exists at the top of the planetary boundary layer, trapping moisture and aerosols (Seibert et al., 2000). Hence, changes in the height of the inversion coincided with the trend of the top of the particulate matter layer on the vertical dimension revealed by MPL.

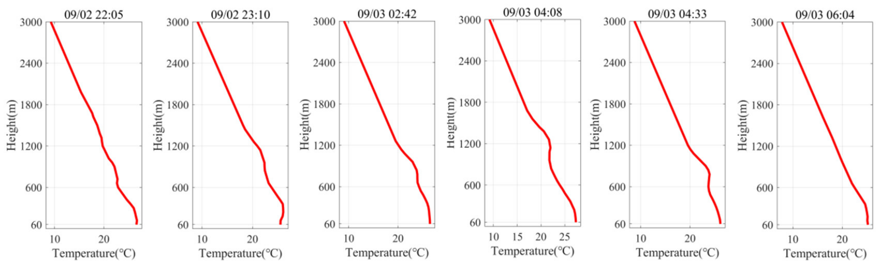

Figure 7. Temperature profiles from the evening of 2 September 2020 to the early hours of 3 September 2020.

3.2.2 Type II: Elevated Single Layer

The particle layer was not only distributed near the ground but sometimes suspended in the air. Figure 8(a) shows the extinction coefficient time series of an elevated single layer of particulate matter. The low extinction coefficient near the ground suggests that it was clean below 400 m in the nighttime. The height of the high extinction coefficient layer gradually rose from 500–800 m at night, which then dropped below 400 m after dawn. The high value of the extinction coefficient corresponded to a higher depolarization ratio than the lower layer, which was approximately 0.02. However, the depolarization ratio of ***Type II*** was significantly lower than the depolarization ratio of the particle layer near the surface of ***Type I***. This differing depolarization ratio was because local emissions dominated in ***Type I***, and the unconverted primary particulate matter with larger particle size accounted for a larger amount than that of ***Type II***.

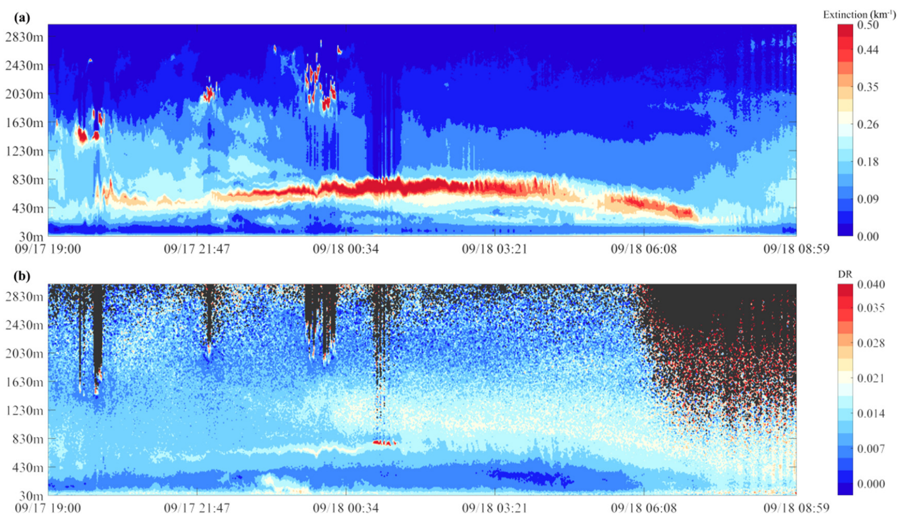

Figure 8. Extinction coefficient at 532 nm (a) and depolarization ratio (b) from 1900 LT 17 on September 2019

https://doi.org/10.5194/acp-2021-457
Preprint. Discussion started: 27 July 2021

to 0859 LT on 18 September 2019.

Figure 9(a) indicated that backward trajectories at 500 m and 100 m were both from near the ground, elevating particles from lower levels vertically. Meanwhile, lower trajectories also carried particles from the upper reaches of the region over Guangzhou horizontally. Wind speed at lower altitudes was relatively low, which was beneficial to regional transport, and allowed particles to stay longer without being blown quickly downstream. In contrast, the trajectory at 1000 m came from a distance in the Yangtze River Delta with a larger wind speed, and the trajectory remained at a high altitude. Particles at 1000 m cannot stay for a long time and were quickly transported downstream by strong winds. Hence, upward airflow near the ground and vertical wind shear at a higher altitude were the causes of particulate matter forming an elevated single layer. Unfortunately, the temperature profile and wind profile data were missing owing to sampling failures. This upward convection of particles was confirmed by the ERA5 vertical velocity reanalysis data of the corresponding time, shown in Figure 10.

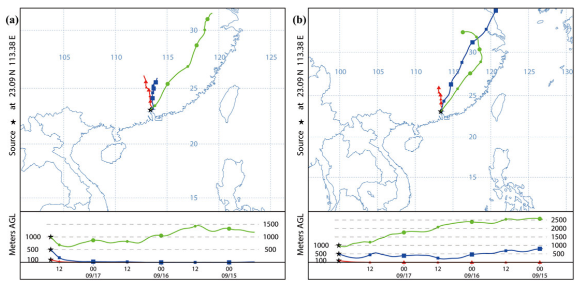

Figure 9. Backward trajectories at 100 m, 500 m, and 1000 m, ending at 2300 LT 17 September 2019 (a) and 0700 LT 18 September 2019 (b), determined by the HYSPLIT model.

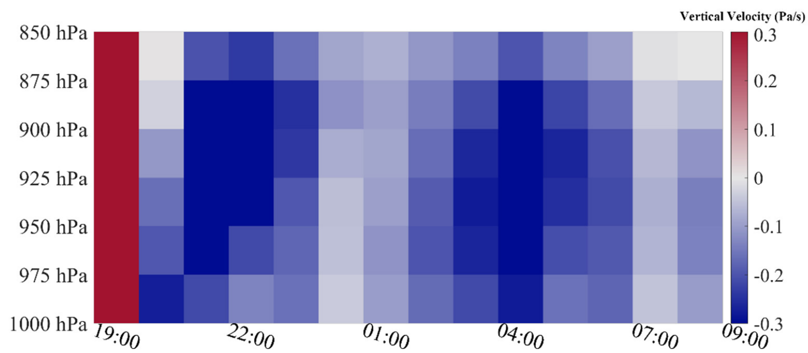

Figure 10. ERA5 hourly vertical velocity from 1900 LT 17 on September 2019 to 0900 LT on 18 September 2019 at 23.25°N, 113.25°E. Negative values indicate upward motion.

https://doi.org/10.5194/acp-2021-457
Preprint. Discussion started: 27 July 2021

3.2.3 Type III: Double Layer

Figure 11 presents a thick single layer of particles transforming into a double layer structure. There was a layer concentrated near the ground after 2300 LT, along with another layer suspended at the height of 600–1000 m. A cleaner layer with a lower extinction coefficient existed between the two-particle layers. The depolarization ratio of the suspending layer was higher than the layer near the surface, especially after 0100 LT, which indicated that sources of the two layers might be different.

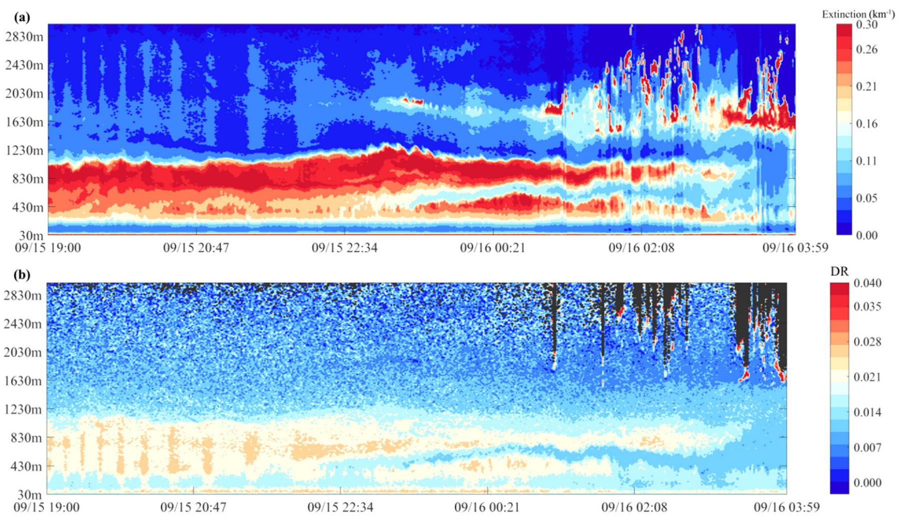

Figure 11. Extinction coefficient at 532 nm (a) and depolarization ratio (b) from 1900 LT 15 on September 2019 to 0359 LT on 16 September 2019.

The vertical distribution of particulate matter was closely related to the horizontal wind speed at various heights (Figure 12). It can be seen that the wind speed of more than 1000 m increased significantly with the altitude, reaching more than 6 m/s. By 2300 LT, the wind speed below 500 m was approximately 4 m/s, obviously higher than the wind speed between 500–1000 m, and there were significant differences in the wind direction. After 2300 LT, the wind speed near the ground decreased, and wind direction gradually turned consistent with the upper level. The wind speed at 500 m continued to be high, reaching 6 m/s maximumly. The layer with higher wind speed corresponded to the height of the cleaner layer, which facilitated the transport of particulate matter downstream in a horizontal direction. Figure 13 illustrates the backward trajectories when the double layer appeared. As shown in Figure 13, the layer of particulate matter below 500 m may have originated in the southwest of the GBA; whereas, the layer of particulate matter at 1000 m may have originated in the Qingyuan and Shaoguan of northern Guangdong.

https://doi.org/10.5194/acp-2021-457
Preprint. Discussion started: 27 July 2021

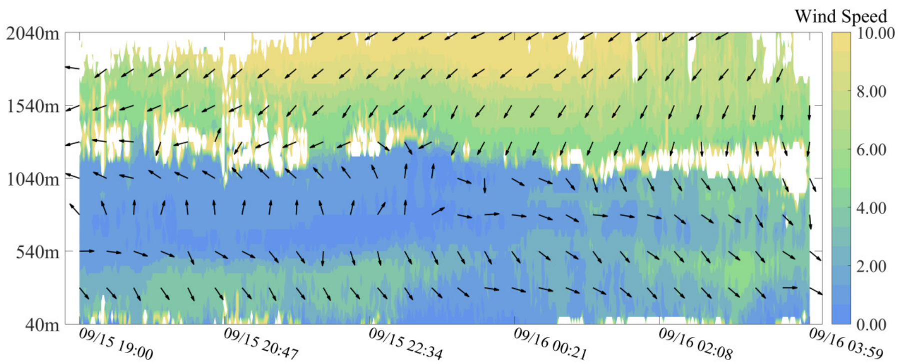

Figure 12. Wind speed and wind direction of Type Ⅲ.

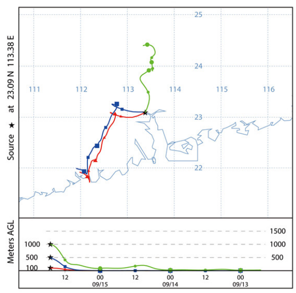

Figure 13. Backward trajectories at 100 m, 500 m, and 1000 m, ending at 0100 LT 16 September 2019, determined by the HYSPLIT model.

The vertical observations of the temperature (Fig. 14.) showed that on the night of 15 September 2019, there was an inversion at 1200 m, which grew thicker. At 0048 LT, like the distribution of the extinction coefficient, the inversion transformed into a double layer structure, with one remaining at 1200 m and another existing under 600 m. The vertical distributed double inversion, which allowed particulate matter to concentrate at the corresponding height, resulted in a double layer distribution of particulate matter.

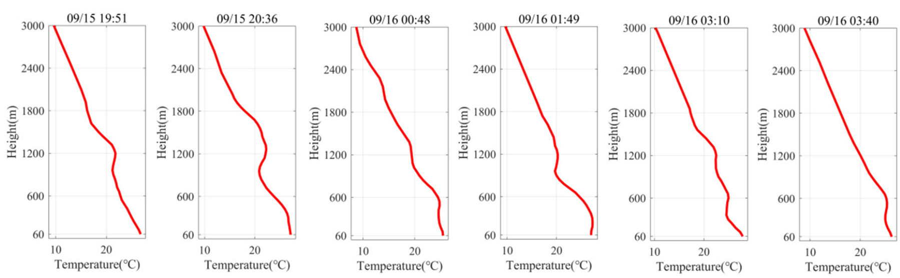

Figure 14. Temperature profiles from the evening of 15 September 2019 to the early hours of 16 September 2019.

https://doi.org/10.5194/acp-2021-457
Preprint. Discussion started: 27 July 2021

Atmospheric Chemistry and Physics Discussions

3.3 Effect of Meteorological Elements on the Distribution of Particles

3.3.1 Extinction Coefficient at Different Wind Speeds

Using data of in situ observations during September and October of 2019 and 2020, statistics of average extinction coefficients at different altitudes and horizontal wind speeds were gathered, as shown in Figure 15. To eliminate the influence of clouds on the extinction coefficient, observations during cloudy weather were manually screened out based on the original signal of the MPL output and images of the sky above the field taken automatically by a camera. The result shows that 500 m was the height with the highest average extinction coefficient, which indicated that the particle layer was most likely to appear at this height. The horizontal wind speed had different effects on the lower and upper parts of the boundary layer. Below 800 m, the extinction coefficient decreased as the wind speed increased, but it was the opposite above 800 m; i.e., the extinction coefficient increased with the wind speed. This altering of the extinction coefficient was because most of the particulate matter in the lower layer came from local emissions and easily accumulated in the presence of a layer with calm wind near the ground. However, in the upper layer, particulate matter was derived more from the surrounding areas, necessitating a certain minimum horizontal wind speed before it could be transported by the wind.

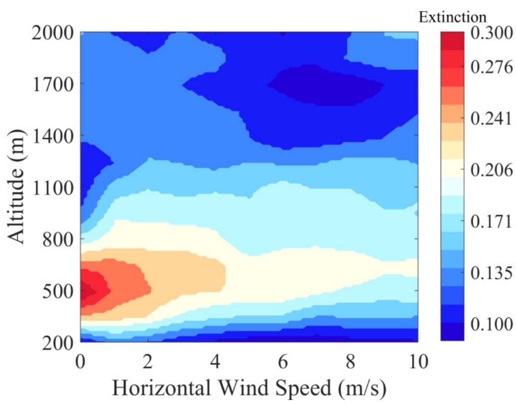

Figure 15. Average extinction coefficient at different wind speeds during September and October of 2019 and 2020.

3.3.2 Conceptual Model of Meteorological Elements and Vertical Distribution of Particles

Based on the observational research above, a conceptual model was developed to summarize the effect of meteorological elements on the three typical vertical distributions of particles in the GBA.

As shown in Figure 16, the surface single layer occurred when calm wind dominated near the ground, which was not conducive to removing particles from local emissions. An elevated single layer was caused by upward airflow near the ground and vertical wind shear at a higher altitude. In this kind of wind structure, particle layer formation was dominated by upward convection and regional transport. A

https://doi.org/10.5194/acp-2021-457
Preprint. Discussion started: 27 July 2021

double layer existed because a layer with stronger horizontal wind existed between two layers with weaker wind, which facilitated the transport of particles from local emission and horizontal transport to downstream areas and resulted in a cleaner layer inside the polluted air mass.

Another key factor that influenced the vertical distribution of particles was temperature inversion, which trapped most anthropogenic emissions from the surface, preventing them from penetrating out of the boundary layer. Furthermore, multiple inversions can cause more than one peak in the concentration of particles vertically.

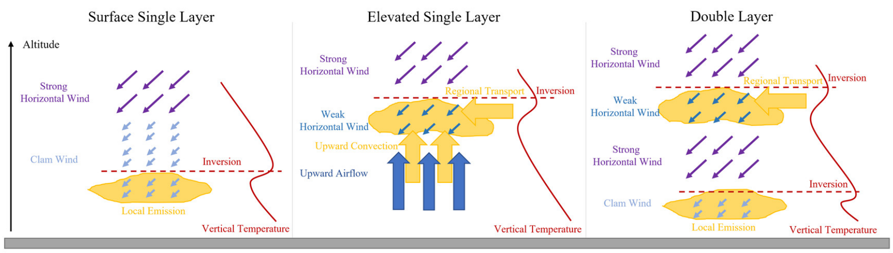

Figure 16. Conceptual model of meteorological elements and vertical distribution of particles.

4. Conclusion

Vehicle-based and in situ multi-lidar observations were conducted during September and October of 2019 and 2020 to study the horizontal and vertical distribution of particles in the GBA. The temperature and wind profiles in the boundary layer were analyzed and confirmed to have a crucial impact on particle distribution characteristics.

The horizontal distribution of particles in the GBA was closely related to wind speed and wind direction. On days with stronger wind in the boundary layer, high values of AOD were mostly distributed in the downstream areas. On days with weaker wind, the horizontal distribution of particles in the GBA presented homogeneously.

The vertical distribution of particles in the GBA was classified into three typical types according to the observations of the MPL: surface single layer, elevated single layer, and double layer. The result of the Doppler wind profile lidar and HYSPLIT backward trajectory model suggested that the sources of the particulate matter of the three types differed. The surface single layer occurred when wind with low speed dominated the boundary layer. The elevated single layer was caused by upward airflow near the ground and vertical wind shear at a higher altitude. The double layer existed because a layer with higher horizontal wind speed existed between two layers with weaker wind. Particles were concentrated near the temperature inversion. Multiple inversions can cause more than one peak in the concentration of particulate matter vertically.

The statistics of average extinction coefficients at different altitudes and horizontal wind speeds revealed the following two mechanisms that affected the distribution of particulate matter in the upper and lower boundary layers. Lower horizontal wind speed was conducive to accumulating particulate matter near the ground. In contrast, higher horizontal wind speed promoted the transport of particles between surrounding areas in the upper boundary layer.

Further studies should be conducted to carry out observations during other seasons in the western Guangdong–Hong Kong–Macao Greater Bay Area to further verify the conceptual model of meteorological elements and vertical distribution of particles proposed in this article. In addition, more vertical observation instruments for meteorological elements, such as a radiometer, could be added to the multi-lidar system to further study the influence of the three-dimensional distribution of humidity, air pressure, and other meteorological elements on the distribution of particles.

Acknowledgments

This work was supported by the National Natural Science Foundation of China (Grant No. 41630422) and Guangdong Major Project of Basic and Applied Basic Research (Grant No. 2020B0301030004).

Data availability. Data available upon request.

Competing interests. The authors declare that they have no conflict of interest.

References

Deng, T., Deng, X., Li, F., Wang, S., and Wang, G.: Study on aerosol optical properties and radiative effect in cloudy weather in the Guangzhou region, Science of the Total Environment, 568, 147−154, https://doi.org/10.1016/j.scitotenv.2016.05.156, 2016.

Du, W., Zhang, Y., Chen, Y., Xu, L., Chen, J., Deng, J., Hong, Y., and Xiao, H.: Chemical characterization and source apportionment of PM2. 5 during spring and winter in the Yangtze River Delta, China, Aerosol and Air Quality Research, 17, 2165−2180, https://doi.org/10.4209/aaqr.2017.03.0108, 2017.

Fang, X., Fan, Q., Li, H., Liao, Z., Xie, J., and Fan, S.: Multi-scale correlations between air quality and meteorology in the Guangdong−Hong Kong−Macau Greater Bay Area of China during 2015–2017, Atmospheric Environment, 191, 463−477, https://doi.org/10.1016/j.atmosenv.2018.08.018, 2018.

Fang, X., Fan, Q., Liao, Z., Xie, J., Xu, X., & Fan, S.: Spatial-temporal characteristics of the air quality in the Guangdong−Hong Kong−Macau Greater Bay Area of China during 2015–2017, Atmospheric Environment, 210, 14−34, https://doi.org/10.1016/j.atmosenv.2019.04.037, 2019.

Fernald, F. G.: Analysis of atmospheric lidar observations: some comments, Applied optics, 23, 652−653, 1984.

Heese, B., Baars, H., Bohlmann, S., Althausen, D., and Deng, R.: Continuous vertical aerosol profiling with a multi-wavelength Raman polarization lidar over the Pearl River Delta, China, Atmos. Chem. Phys., 17, 6679–6691, https://doi.org/10.5194/acp-17-6679-2017, 2017.

Leikauf, G. D., Kim, S. H., and Jang, A. S.: Mechanisms of ultrafine particle-induced respiratory health effects, Experimental & Molecular Medicine, 52, 329–337, https://doi.org/10.1038/s12276-020-0394-0, 2020.

Li, Y., Wang, B., Lee, S. Y., Zhang, Z., Wang, Y., and Dong, W.: Micro-Pulse Lidar Cruising Measurements in Northern South China Sea, Remote Sensing, 12, 1695, https://doi.org/10.3390/rs12101695, 2020.

Liao, Z., Gao, M., Sun, J., and Fan, S.: The impact of synoptic circulation on air quality and pollution-related human health in the Yangtze River Delta region, Science of the Total Environment, 607, 838−846, https://doi.org/10.1016/j.scitotenv.2017.07.031, 2017.

Liu, J., Wu, D., Fan, S., Mao, X., and Chen, H.: A one-year, on-line, multi-site observational study on water-soluble inorganic ions in $PM_{2.5}$ over the Pearl River Delta region, China, Science of the Total Environment, 601, 1720−1732, https://doi.org/10.1016/j.scitotenv.2017.06.039, 2017.

Liu, Q., He, Q., Fang, S., Guang, Y., Ma, C., Chen, Y., Kang, Y., Pan, H., Zhang, H., and Yao, Y.: Vertical distribution of ambient aerosol extinctive properties during haze and haze-free periods based on the Micro-Pulse Lidar observation in Shanghai, Science of the Total Environment, 574, 1502−1511, https://doi.org/10.1016/j.scitotenv.2016.08.152, 2017.

Lu, X., Mao, F., Pan, Z., Gong, W., Wang, W., Tian, L., and Fang, S.: Three-dimensional physical and optical characteristics of aerosols over central china from long-term CALIPSO and HYSPLIT data, Remote Sensing, 10, 314, https://doi.org/10.3390/rs10020314, 2018.

Lv, L., Liu, W., Zhang, T., Chen, Z., Dong, Y., Fan, G., Xiang, Y., Yao, Y., Yang, N., Chu, B., Teng, M., and Shu, X.: Observations of particle extinction, $PM_{2.5}$ mass concentration profile and flux in north China based on mobile lidar technique. Atmospheric Environment, 164, 360−369, https://doi.org/10.1016/j.atmosenv.2017.06.022, 2017.

Lyu, L., Dong, Y., Zhang, T., Liu, C., Liu, W., Xie, Z., Xiang, Y., Zhang, Y., Chen, Z., Fan, G., Zhang, L., Liu, Y., Shi, Y., and Shu, X.: Vertical Distribution Characteristics of $PM_{2.5}$ Observed by a Mobile Vehicle Lidar in Tianjin, China in 2016, Journal of Meteorological Research, 32, 60−68, https://doi.org/10.1007/s13351-018-7068-z, 2018.

Kim, H. C., Chai, T., Stein, A., and Kondragunta, S.: Inverse modeling of fire emissions constrained by smoke plume transport using HYSPLIT dispersion model and geostationary satellite observations, Atmos. Chem. Phys., 20, 10259−10277, https://doi.org/10.5194/acp-20-10259-2020, 2020.

Orru, H., Ebi, K. L., and Forsberg, B.: The interplay of climate change and air pollution on health, Current environmental health reports, 4, 504−513, https://doi.org/10.1007/s40572-017-0168-6, 2017.

Seibert, P., Beyrich, F., Gryning, S. E., Joffre, S., Rasmussen, A., and Tercier, P.: Review and intercomparison of operational methods for the determination of the mixing height, Atmospheric Environment, 34, 1001−1027, https://doi.org/10.1016/S1352-2310(99)00349-0, 2000.

Shao, Q., Liu, X., and Zhao, W.: An alternative method for analyzing dimensional interactions of urban carrying capacity: case study of Guangdong−Hong Kong−Macao Greater Bay Area, Journal of Environmental Management, 273, 111064, https://doi.org/10.1016/j.jenvman.2020.111064, 2020.

Stocker, T. (Ed.): Climate change 2013: the physical science basis: Working Group I contribution to the Fifth assessment report of the Intergovernmental Panel on Climate Change, Cambridge university press, 2014.

Strawa, A. W., Kirchstetter, T. W., Hallar, A. G., Ban-Weiss, G. A., McLaughlin, J. P., Harley, R. A., and Lunden, M. M.: Optical and physical properties of primary on-road vehicle particle emissions and their implications for climate change, Journal of Aerosol Science, 41, 36–50, https://doi.org/10.1016/j.jaerosci.2009.08.010, 2010.

Tian, P., Cao, X., Zhang, L., Sun, N., Sun, L., Logan, T., Shi, J., Wang, Y., Ji, Y., Lin, Y., Huang, Z., Zhou, T., Shi, Y., and Zhang, R.: Aerosol vertical distribution and optical properties over China from long-term satellite and ground-based remote sensing, Atmos. Chem. Phys., 17, 2509–2523, https://doi.org/10.5194/acp-17-2509-2017, 2017.

Wallace, J., and Kanaroglou, P.: The effect of temperature inversions on ground-level nitrogen dioxide (NO_2) and fine particulate matter ($PM_{2.5}$) using temperature profiles from the Atmospheric Infrared Sounder (AIRS), Science of the Total Environment, 407, 5085−5095, https://doi.org/10.1016/j.scitotenv.2009.05.050, 2009.

Xie, J., Liao, Z., Fang, X., Xu, X., Wang, Y., Zhang, Y., Liu, J., Fan, S., and Wang, B.: The characteristics of hourly wind field and its impacts on air quality in the Pearl River Delta region during 2013–2017, Atmospheric Research, 227, 112−124, https://doi.org/10.1016/j.atmosres.2019.04.023, 2019.

Xu, Y., Xue, W., Lei, Y., Zhao, Y., Cheng, S., Ren, Z., and Huang, Q.: Impact of meteorological conditions on $PM_{2.5}$ Pollution in China during winter, Atmosphere, 9, 429, https://doi.org/10.3390/atmos9110429, 2018.

Yao, L., Zhan, B., Xian, A., Sun, W., Li, Q., and Chen, J.: Contribution of transregional transport to particle pollution and health effects in Shanghai during 2013–2017, Science of the Total Environment, 677, 564-570, https://doi.org/10.1016/j.scitotenv.2019.03.488, 2019.s

https://doi.org/10.5194/acp-2021-457
Preprint. Discussion started: 27 July 2021

Zang, Z., Wang, W., You, W., Li, Y., Ye, F., and Wang, C.: Estimating ground-level $PM_{2.5}$ concentrations in Beijing, China using aerosol optical depth and parameters of the temperature inversion layer, Science of the Total Environment, 575, 1219−1227, https://doi.org/10.1016/j.scitotenv.2016.09.186, 2017.

Zhou, Y., Shan, Y., Liu, G., and Guan, D.: Emissions and low-carbon development in Guangdong-Hong Kong-Macao Greater Bay Area cities and their surroundings, Applied energy, 228, 1683−1692, https://doi.org/10.1016/j.apenergy.2018.07.038, 2018.